

Spatially dependent multiphoton multiple ionization

P. Hansch, M. A. Walker, and L. D. Van Woerkom

Department of Physics, The Ohio State University, Columbus, Ohio 43210

(Received 5 June 1996)

We have measured spatially dependent multiple ionization of xenon in an intense ultrashort pulse laser field. The ion yields for various charge states are dramatically different due to selecting specific locations within a Gaussian laser focus. The data show a clear enhancement of higher charge states and the double ion exceeds the single ion yield at certain locations. A model based on space-dependent volume scaling for different charge states is presented. [S1050-2947(96)50710-9]

PACS number(s): 32.80.Rm, 32.80.Fb

Photoelectron and ion spectroscopy at high laser intensities (above 10^{12} W/cm²) is currently studied by many groups in physics, chemistry, and materials research in order to uncover the fundamental mechanisms of laser-matter interaction. Among the long-term goals of these research efforts is the achievement of coherent control, i.e., controlling atoms and molecules with light. One of the major difficulties plaguing strong field control efforts is the continuous distribution of intensities contained within a typical laser focal volume. Intensity-dependent phenomena are “blurred” by the spatial averaging inherent in tightly focused geometries. This Rapid Communication presents measurements of multiple ionization coming from greatly reduced spatial extent. It is shown that the ionization results from spatial regions characterized by only a radial intensity dependence. The key features of these measurements are (1) enhanced detection of high-intensity effects, (2) improved signal-to-noise ratio by blocking out low-intensity regions in the focal volume, (3) reduction of complex intensity distribution to a one-dimensional radial dependence within a selected window, and (4) precise peak intensity control while maintaining good overall beam quality.

Given the sensitive intensity control, it is possible to measure the evolution of ionization rates for multiple charge states of atoms and molecules as a function of intensity, simplifying the effects of spatial averaging over a continuously changing ionization volume. Traditionally, ionization rates at different high intensities have been studied by reducing the overall peak intensity of a focused laser beam. Ionization spectra have been regarded as being dominated by the strong field interaction near the absolute peak intensity at the minimum beam waist. As we will demonstrate in this paper a non-negligible fraction of xenon ions can be generated as far as several Rayleigh ranges away from the minimum beam waist. Typically, the entire ionization volume is exposed to the time-of-flight detector. For a given ion charge state the ion yield after saturation continues to rise as the intensity increases due to the growth of the entire focal volume [1,2]. The true ionization rates (intensity-dependent, not volume-dependent) can only be extracted by deconvolving the complicated Gaussian volume. Despite the low ionization rates at low intensities, the volume increase in a Gaussian focal volume causes a significant number of ions to be produced far away from the center of the beam.

Previously, Jones [3] demonstrated spatially selective ion spectroscopy using a large unfocused beam and a large aperture. In contrast, the present work exploits a tight focusing geometry and a very small aperture. This allows the study of a broader range of intensities under otherwise identical conditions, while the intensity distribution within a selected window is very well known.

We applied intensity-selective scanning (ISS) to obtain the presented ion spectra. As previously demonstrated by Hansch and Van Woerkom [4], intensity-selective photoelectron spectroscopy can be studied by combining high-repetition-rate laser technology and the optical properties of focused laser beams. In order to avoid a spatially averaged ion signal, only a very small fraction of the ionization region is exposed to the detector. Unlike photoelectrons, ions must be accelerated toward the detector to record time-of-flight data. Therefore, ionization occurs in the presence of a static electric field oriented such that ions are swept toward and electrons away from the detector, as shown in Fig. 1. The entire flight tube is at ground potential and the grid opposing the pinhole has a potential of +1100 V. By moving the focusing lens via a translation stage, the focal volume can be scanned across the pinhole exposing only a thin “slice” of the ionization region rather than the whole volume. A pinhole diameter of 500 μ m justifies treating the exposed volume as a slice since the beam diameter near the focal region is only several times 10 μ m. Therefore, the round pinhole acts effectively as a slit. The observed volume can be well described as cylindrically symmetric within the width of the pinhole with only a radial intensity dependence that is well known as a function of r and z . The spatial distribution of the

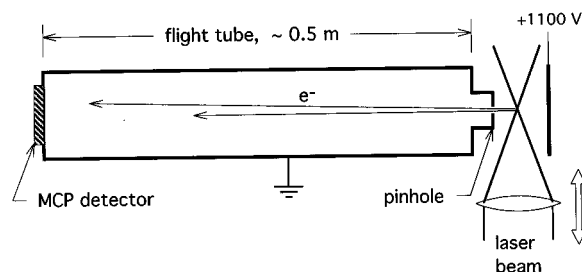


FIG. 1. Schematic setup of the time-of-flight spectrometer. The focusing lens can be moved via a translation stage to scan the ionization volume across the pinhole at the front of the flight tube.

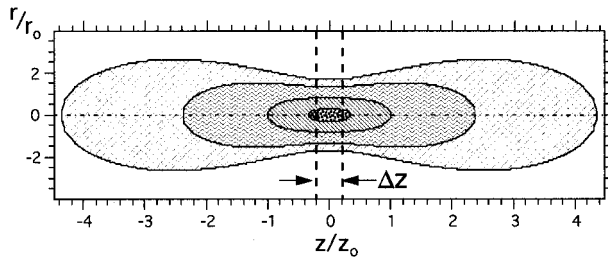


FIG. 2. Schematic intensity contours. Low intensities occupy a much larger volume than high intensities in comparison to the ISS technique.

temporal peak intensities in a Gaussian laser focus is Lorentzian in z and Gaussian in r , given by

$$I(r, z) = I_0 \left(\frac{r_0}{\omega(z)} \right)^2 \exp \left[-2 \left(\frac{r}{\omega(z)} \right)^2 \right], \quad (1)$$

where I_0 is the maximum intensity at the spatial and temporal peak and r_0 is the minimum waist size for the electric field. The z -dependent waist is given by $\omega(z) = r_0 \sqrt{1 + (z/z_0)^2}$, where z_0 is the Rayleigh range given by $z_0 = \pi r_0^2 / \lambda$. Figure 2 shows the schematic scaling of several iso-intensity contours according to Eq. (1). The largest fraction of the total Gaussian focal volume is occupied by low intensities. In contrast, ISS uses the pinhole of width Δz to select a slice of the focal region where the volumetric weighting enhances high-intensity regions by blocking most of the low-intensity volume.

The presented ion spectra have been generated using a 1-kHz Ti:sapphire laser system, producing 100-fs, 800-nm pulses with an energy of 700 μJ per pulse and plane polarized. A telescope serves to enlarge the beam diameter, and with a 25-cm focal length lens an absolute intensity of $I_0 = 4 \times 10^{14} \text{ W/cm}^2$ can be reached inside the interaction chamber. The focus is further characterized by a minimum waist radius $r_0 = 17 \mu\text{m}$. The vacuum chamber has a base pressure of 2×10^{-10} torr and was backfilled with xenon to 6×10^{-9} torr to record ion spectra. The ion time-of-flight signal was detected with a pair of microchannel plates. A multichannel analyzer (MCA) recorded events in successive 5-ns-time bins. The low xenon pressure was chosen to avoid pulse pileup in the MCA. In the case of photoelectron spectroscopy only a small fraction of the emitted electrons is detected due to their angular distribution. In our case *all* ions are swept toward the detector and a lower pressure suffices to maintain good count rates while avoiding space charges. The reported spectra have been acquired with typically 5×10^5 laser pulses per scan.

Figure 3 shows a xenon ion signal that has been converted from time-of-flight to atomic mass, including proper scaling through the Jacobian of the time-mass transformation. A time-of-flight spectrometer can only differentiate between ions with different q/m . Therefore, Xe^+ ions are located at the neutral Xe mass around 132 amu, while Xe^{2+} , Xe^{3+} , and Xe^{4+} appear at 1/2, 1/3, and 1/4 the neutral mass, respectively. Each charge state shows a group of lines that correspond to the different isotopes of xenon. The most prominent isotopes range from ^{128}Xe to ^{136}Xe and can be very well resolved. Figure 3 contrasts (a) the traditional method of ex-

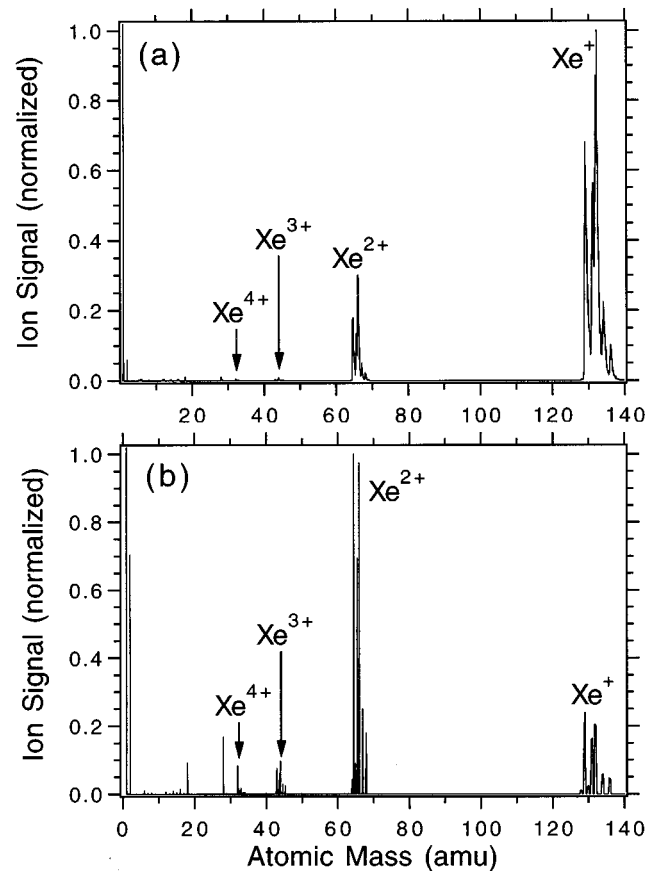


FIG. 3. Xenon-ion spectra recorded using (a) a traditional method of exposing entire focal volume vs (b) selecting a 500- μm window with ISS at the minimum beam waist.

posing the full ionization volume vs (b) intensity-selective scanning, exposing only the minimum beam waist. Both spectra have been normalized for comparison. It is apparent that the single ions dominate the spectrum in (a), followed by a significantly smaller fraction of double ions. The Xe^{3+} and Xe^{4+} counts on the other hand are close to the noise level, and their contributions are almost negligible compared to Xe^+ . The reason Xe^+ yields the maximum contribution is that single ions are generated within a much larger volume than any of the higher charge states. For absolute peak intensities I_0 that are greater than the saturation intensity to create Xe^+ , the spatial weighting factor grows as $I_0^{3/2}$ [1]. The higher charge states are only produced near the core of the Gaussian focal volume, since they require higher intensities. The volumetric weighting results in an enhancement of single ions. Furthermore, the large-volume, low-intensity regions of the laser focus introduce much noise by ionizing contaminants with typically low ionization potentials. The spatial weighting makes it difficult for highly charged ions coming from small volumes to compete with these large-volume noise contributions, and introduces significant uncertainties when trying to extract quantitative ionization rates for high charge states.

In contrast, Fig. 3(b) shows an ISS ion spectrum where the pinhole exposed only the peak intensity region at the minimum beam waist. Due to the spatial selectivity, the various charge states of Xe have different volumetric weightings

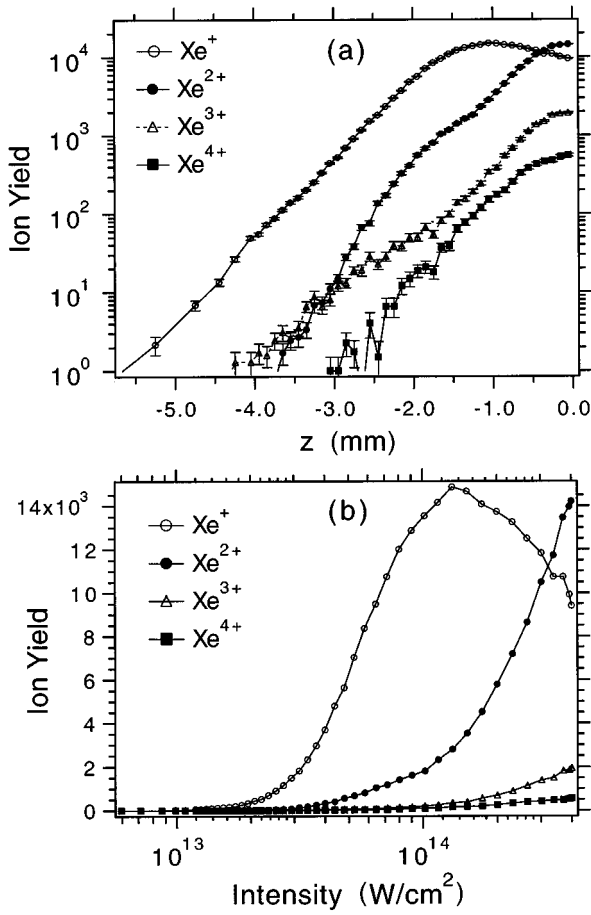


FIG. 4. (a) Ion signal of xenon with 800-nm, 140-fs pulses as a function of z ; (b) same signal displayed vs local on-axis peak intensity.

and now the Xe^{2+} ions dominate the spectrum, followed by Xe^+ and clearly enhanced contributions from Xe^{3+} and Xe^{4+} . Since the overall count rates drop by limiting the view with the pinhole, only the relative signals are meaningful in terms of enhancements. Moreover, it should be noted that the ISS technique yields better isotope resolution and a reduction of noise, such that Xe^{3+} and Xe^{4+} can unambiguously be identified. The single ion signal is not as prominent anymore, since the contributions from low-intensity regions far away from the core are blocked out. Within the selected window the number of Xe^+ ions is saturated, and sequential ionization starts depleting these single ions to produce Xe^{2+} and higher charge states. By simplifying the complex overall intensity distribution to a slice, which is approximately cylindrically symmetric and only has a radial intensity dependence, a much cleaner measurement of high-intensity effects can be obtained. Particularly, low-probability events can be observed by reducing the noise.

The peak intensity within a spatially selected part of the laser focus can be varied by selecting different slices along the z axis (the direction of propagation of the laser beam), as shown in Fig. 4(a). Starting at the minimum beam waist the laser focus was scanned across the pinhole in 100- μm steps over a range of nearly 6 mm (~ 8 Rayleigh ranges). Figure 4(a) displays the number of detected ions for the various charge states as a function of z along the beam axis. In order

to qualitatively demonstrate the trends, different detection efficiencies for different Xe charge states are not taken into account. For any selected z position the local on-axis peak intensity can be obtained via Eq. (1) as

$$I(r=0,z) = \frac{I_0}{1+z^2/z_0^2}. \quad (2)$$

Using Eq. (2) with $I_0 = 4 \times 10^{14}$ W/cm² and $z_0 = 0.7$ mm, the recorded evolution of ion counts from Fig. 4(a) can be converted to signal vs local peak intensity, as shown in Fig. 4(b). In addition to a more balanced volumetric weighting, ISS provides another important advantage: By moving along z , different peak intensities can be selected *without* changing the nature of the laser beam. Traditionally, the absolute intensity I_0 had to be changed when exposing the full volume. Inserting additional optics into the beam to control I_0 may result in affecting the overall beam quality and temporal width of the pulses. With ISS these problems can be avoided.

Figure 4(b) shows that the highest number of Xe^+ is not produced at the absolute peak intensity, instead it peaks near the saturation intensity of the double ions. When looking at the full volume the signal is characterized by a change in slope at the saturation intensities and a continued rise according to $I_0^{3/2}$ [2]. By using ISS, the saturated volume stays nearly constant with no increase in the total number of atoms that can be ionized. When moving toward the center of the beam, higher intensities become available without increasing the width of the observed slice. This leads to depletion of Xe^+ and a sharp rise in Xe^{2+} . At the same time, the rates for sequentially producing higher charge states rise as well. Further calculations are currently underway to quantitatively extract intensity-dependent ionization probabilities from the measured data. The analysis of ionization probabilities benefits significantly from the simplified geometry, as is planned to be demonstrated in a future publication [5].

It is well known that for a Gaussian focus with absolute intensity I_0 the total volume occupied by intensities greater than some saturation intensity I_s is given by [6]

$$V(I_s, I_0) = \pi z_0 \omega_0^2 \left\{ \frac{4}{3} \left[\frac{I_0 - I_s}{I_s} \right]^{1/2} + \frac{2}{9} \left[\frac{I_0 - I_s}{I_s} \right]^{3/2} - \frac{4}{3} \tan^{-1} \left[\frac{I_0 - I_s}{I_s} \right]^{1/2} \right\}. \quad (3)$$

For absolute intensities I_0 much greater than the saturation intensity I_s of a given charge state, Eq. (3) yields the familiar volume increase according to $I_0^{3/2}$. It should be noted that, to be exact, the volume generating a given ion charge state equals the corresponding total $V(I_s, I_0)$ minus the saturated volume of higher charge states. However, when exposing the full focal region, this difference becomes negligible. For instance, the full saturation intensity contour will always be significantly larger for Xe^+ than for Xe^{2+} , etc.

For intensity-selective scanning, on the other hand, one *must* consider the differences between consecutive saturation volumes due to their comparable size. The volume slice that experiences intensities greater than some I_s is given by

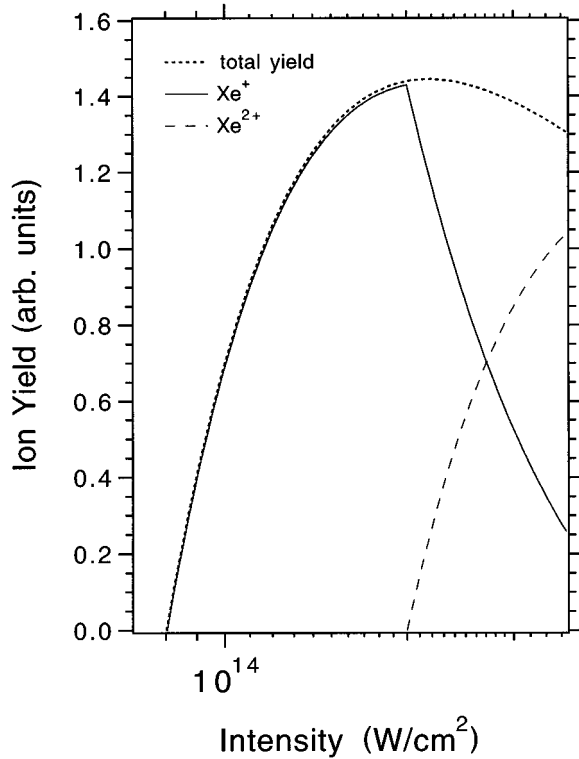


FIG. 5. Calculated volumes for saturated ionization for single and double ions. The model predicts the single ion yield to decrease as the intensity increases due to the creation of higher charge states.

$$V_{\text{ISS}}(I_s, I_0, I_{0L}) = \frac{1}{2} \pi \omega_0^2 \Delta z \frac{I_0}{I_{0L}} \ln\left(\frac{I_{0L}}{I_s}\right), \quad (4)$$

where I_0 is the absolute peak intensity, I_{0L} is the local on-axis peak intensity at a given z position according to Eq. (2), and Δz is the pinhole diameter. Under the approximation that volumes with saturated intensities dominate the ion signal, Fig. 5 displays the calculated ion yields based on Eq. (4), with saturation intensities of $I_s(\text{Xe}^+) = 8 \times 10^{13} \text{ W/cm}^2$ and $I_s(\text{Xe}^{2+}) = 2 \times 10^{14} \text{ W/cm}^2$, and an absolute peak intensity of $I_0 = 4 \times 10^{14} \text{ W/cm}^2$. It is apparent that the effective volume

producing single ions starts dropping as soon as the saturation intensity for double ions is reached. Moving in z toward the minimum beam waist increases the local peak intensity I_{0L} without increasing the total ionized volume. In fact, due to the bone-shaped intensity contours, as shown in Fig. 2, the total number of ionized atoms decreases slightly when reaching the core of the focus, as indicated by the dotted line in Fig. 5, which represents the total yield of all charge states. The volumetric model based on Eq. (4) captures the ionization process at the high-intensity end sufficiently well. It clearly demonstrates how the production of double ions burns a hole into the total volume capable of generating single ions. The Xe^{3+} and Xe^{4+} signals have not been included in Fig. 5, since those charge states are clearly not saturated yet. Of course, the above model of saturated volumes cannot reproduce the low-intensity features of our experimental data in Fig. 4(b). The tails below the saturation intensities arise from nonresonant ionization with low probabilities, and traditionally follow an I^n dependence, n being the number of absorbed photons. For higher than single charge states nonsequential ionization also contributes.

In conclusion we have observed strong field multiple ionization with a much more balanced volumetric weighting of the intensities producing up to quadruple ions in xenon. Intensity-selective scanning yields a cleaner signal and better signal-to-noise ratios by blocking out large-volume low-intensity contributions. The observed peak intensities can be controlled very accurately by moving the pinhole along z . ISS will be an essential tool in extracting real ionization rates because the volumetric scaling is easier to deconvolve and the intensity distribution has been simplified to only a radial dependence. Future improvements in the ISS design include reducing the window size to only a few times $10 \mu\text{m}$ to minimize the effects of spatial averaging within the window width. The use of kilohertz short-pulse lasers will maintain reasonable count rates, despite the reduced volume exposure. In addition, properly shaped pulses can eliminate the temporal intensity variation of the observed ionization.

This material is based upon work supported by (or in part by) the U.S. Army Research Office under Grant No. DAAH04-95-1-0418.

- [1] A. l'Huillier, L. A. Lompre, G. Mainfray, and C. Manus, Phys. Rev. A **27**, 2503 (1983).
 [2] B. Walker *et al.*, Phys. Rev. Lett. **73**, 1227 (1994).
 [3] R. R. Jones, Phys. Rev. Lett. **74**, 1091 (1995).
 [4] P. Hansch and L. D. Van Woerkom, Opt. Lett. **21** 1286 (1996).

- [5] M. A. Walker, P. Hansch, and L. D. Van Woerkom (unpublished).
 [6] G. N. Gibson, R. R. Freeman, T. J. McIlrath, and H. G. Muller, Phys. Rev. A **49**, 3870 (1994).